Photoacoustic Registration and Visualization

Project Report
600.446 Computer Integrated Surgery II Spring 2012
Group 9: Alexis Cheng
Mentors: Professors Russell Taylor, Emad Boctor, and Jin U. Kang

Abstract. Interventional guidance systems require surgical navigation systems to register different tools and technologies together. Standard navigation systems have drawbacks leading to target registration errors (TRE) of around 3mm. This project introduces the photoacoustic (PA) effect as a direct 3D ultrasound (US) to video registration method. We demonstrate its feasibility on both a synthetic phantom and an ex-vivo liver tissue phantom. We achieve an average TRE of 0.8 mm on a synthetic phantom and an average TRE of 1.1 mm on the ex-vivo tissue phantom. We highlight the technical approach to enable this registration method and propose future work to be done.

1. Introduction

PA registration has been shown to be a promising alternative to common surgical tracking systems such as electromagnetic or optical trackers [1]. This registration system involves projecting a series of laser points onto a phantom or tissue surface that can be seen by a stereovision camera system. The laser energy is absorbed by the phantom or tissue and generates an acoustic wave that can be detected by conventional ultrasound transducers.

This project aims to develop a PA registration and visualization system that can perform a direct registration from 3D stereo-camera (SC) space to 3D ultrasound (US) space in a synthetic phantom and an ex-vivo tissue environment whilst achieving sub-millimeter target registration error (TRE) results.

Significance and Motivation

Interventional guidance systems are very common in modern surgical procedures including laparoscopic surgery and robotic surgery [3]. These guidance systems are used because it may be difficult to locate important structures such as tumours both due to its movement during the procedure or the camera's limited field of view. The systems typically provide information support with overlays of other imaging modalities onto the video. Before use, they must be registered with a number of surgical tools and technologies. This step is commonly accomplished using electromagnetic (EM) or optical surgical navigation systems [4, 5].

There are several drawbacks associated with these standard surgical navigation systems. They require trackable markers to be placed on the tools of interest such as an ultrasound transducer. To actually obtain the transformation from the camera space to the ultrasound image space, a calibration is necessary to determine the transformation from the tracked marker to the ultrasound image. This calibration is a significant source of error and is a large area of research [6, 7]. They have demonstrated errors around 3mm [6, 8, 9].

Background

The PA effect was observed in 1880 by Alexander Graham Bell. The general principle of this phenomenon is that light waves can generate an acoustic wave when absorbed by matter due to thermal absorption and excitation. It was initially developed for the communication field, but has since

been used in the medical field as well such as PA spectroscopy. This biomedical application is mainly used for functional and structural imaging thanks to the large contrast in absorption coefficients between blood and tissue [2].

When matter is exposed to pulses of light, the light energy becomes absorbed by the molecules within the matter. The absorbed energy thermally excites the molecules and generates heat. This causes the matter to expand and will generate an acoustic wave if the absorbed energy exceeds a certain threshold. These waves can be detected by an assortment of acoustic devices such as ultrasound transducers.

Previous work [1] demonstrated the proof of concept that a registration between SC space and 2D US space could be obtained using this technique. This system addresses the drawbacks of standard EM or optical surgical navigation systems. First, markers are unnecessary since the projected laser points can be seen in the video and can also generate an effective PA signal in the 3D US volume [10, 11, 12, 13]. Second, the projected laser points are already resolved as 3D points in the frames that we are interested in. The laser spots can be seen as green points in the video images and as a PA signal in the 3D US volume. The 3D point sets in these two frames can be directly registered using rigid registration techniques [4, 5, 14].

Goal

The goal of this project is to develop a PA registration and visualization system that can directly register 3D video with 3D US. We deliver a procedure for collecting data, an initial design of a fiber delivery system, a software pipeline for segmenting laser points from the video, a software pipeline for segmenting PA points from the US volume, a software pipeline for calculating the TRE, and a preliminary visualization of what the final visualization may look like. We also present experimental results of our system performance on a synthetic phantom and an ex-vivo phantom. Finally, we discuss our results and present future directions for this work.

2. Technical Approach

To conduct our experiments, we use a Q-switched neodymium-doped yttrium aluminum garnet (Nd:YAG), Brilliant (Quantel Laser, France) laser frequency doubled to 532nm wavelength at 14mJ/cm^2 to generate a PA effect on the synthetic phantom and the ex-vivo tissue phantom. Most of the laser energy is absorbed at the superficial surface of the tissue. However, there is a non-zero amount of penetration into the tissue, creating a source of error that will be discussed. Our stated energy is lower than the maximum allowable energy of 30 mJ/cm^2 exposed on tissue as per the ISO laser safety standards. We use a SonixCEP US system along with a 4DL14-5/38 US transducer developed by Ultrasonix Medical Corporation (Richmond, Canada) to scan the volume of interest. The motor actuation of this transducer induces angular movement around an internal pivot point. The Sonix DAQ device, developed in collaboration between the University of Hong Kong and Ultrasonix, is used to acquire pre-beamformed radiofrequency (RF) data directly from the US machine. We use the k-wave toolbox [15] in MATLAB (Mathworks Inc. Natick, MA) designed for PA reconstruction. A custom-built SC system containing 2 CMLN-13S2C cameras (Point Grey Research, Richmond, Canada) is used to capture images to be used for 3D triangulation. The synthetic phantom is made using plastisol and black dye. The ex-vivo liver phantom is made using a gelatin solution and a porcine liver. The surface of the kidney is partially exposed and not covered by gelatin.

The following sections will give details on: a procedure for collecting data, an initial design of a fiber delivery system, a software pipeline for segmenting laser points from the video, a software pipeline

for segmenting PA points from the US volume, a software pipeline for calculating the TRE, and a preliminary visualization of what the final visualization may look like.

Data Collection

Figure 1 shows the procedure for collecting data. Step 1 is when we project the laser points onto the phantom. This requires us to place the laser point using mirrors to redirect the laser beam. We also use an iris to partially occlude the 6mm diameter laser beam resulting in a 1mm diameter laser beam. In step 2, we take several camera images from the left camera and the right camera. The camera has a faster frame rate than the laser system, thus some of the images have the laser point and other images only have the background. We will exploit this in the laser point segmentation pipeline.

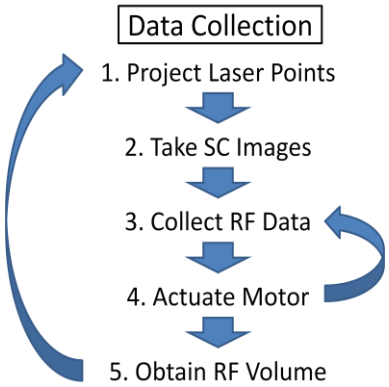

Figure 1. Data Collection Procedure

Steps 3 and 4 are part of an iterative process. Our current setup requires us to manually actuate the transducer motor to obtain ultrasound images for each individual slice. Ideally, we will synchronize the motor actuation and the RF data collection so that we can iterate steps 3 and 4 automatically. The number of times that we iterate depends on the number of slices we desire in our US volume. Future studies could look at optimizing between more slices for a finely sampled volume versus fewer slices for faster data acquisition. Step 5 collects the data collected in steps three and four into a single folder. This whole process is iterated for the number of laser points that we intend to collect. This is something that we will replace with a fiber delivery system that can project multiple points concurrently.

Fiber Delivery

A fiber delivery systems involves first splitting the beam into multiple projected spots and to collimate the output of these beams such that the spots remain a constant size regardless of the distance to the tissue. A way to accomplish this is to couple the laser beam with a fiber bundle. We can then split the bundle of fibers at the output end to get multiple laser spots. Figure 2 is a beamformed US slice where multiple points are present. It should be noted that the fiber output was placed very close to the tissue because fiber output collimation is still in development. We have tried many different combinations of fiber and lens to no avail. We continue to look for a combination of fiber and lens that result in successful beam collimation.

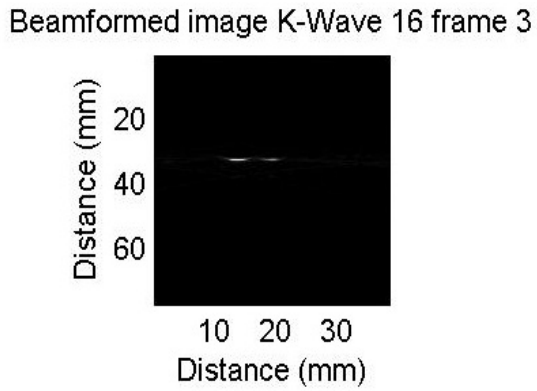

Figure 2. Multiple laser spots in a single US slice

Video Segmentation

Figure 3 shows the pipeline used for the segmentation of laser points in the SC images. As mentioned before, we have multiple frames for each of the cameras, some of which have the laser point and others do not. This allows us to perform step one to obtain a difference image which makes it much simpler to segment the laser point. Figure 4 gives an example of a SC image and the difference image.

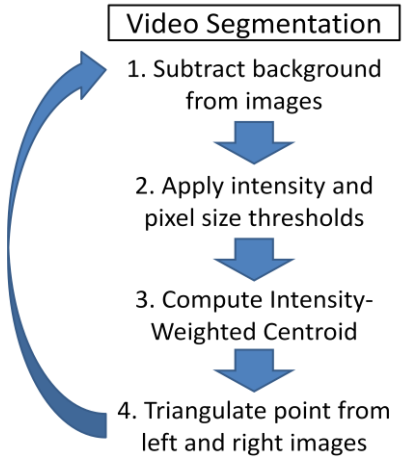

Figure 3. Software Pipeline for Segmentation of Laser Points in Video

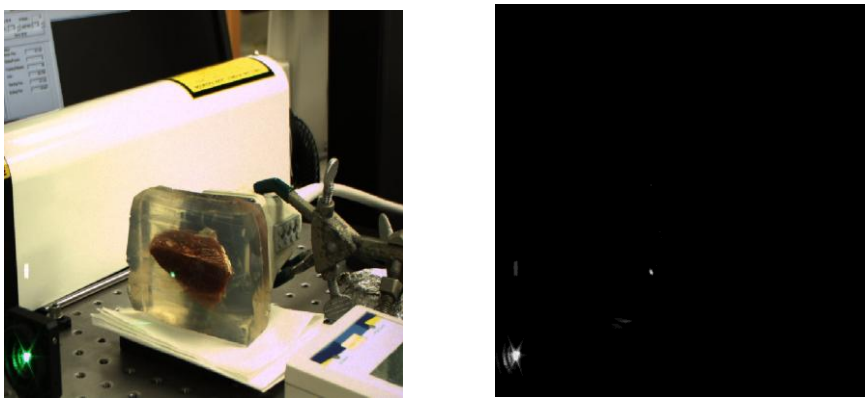
Figure 4. Examples of a SC image and a difference SC image

Step 2 is a combination of an intensity threshold filter, a pixel size threshold filter, and a region shape filter. We take advantage of the fact that our phantom is in the middle of the images and disregard the borders of the image. The main reason for doing this is the presence of the iris which generates another laser point that we are not interested in. The intensity threshold is chosen such that if the normalized pixel intensity is less than 0.3, then it becomes 0. On the other hand, if it is equal or greater than 0.3, it becomes 1. This threshold is selected experimentally and will differ based on the laser intensity. The pixel size threshold is chosen such that regions with very few pixels or a lot of pixels are rejected. These bounds depend greatly on the beam size and the reflectivity of the tissue. For example, the same beam size could have a much larger spot if the tissue is very reflective. Finally, the shape filter is applied because the laser occasionally generates a line artifact. To do this, we enforce that the elliptical point region has major and minor axes within five pixels of each other.

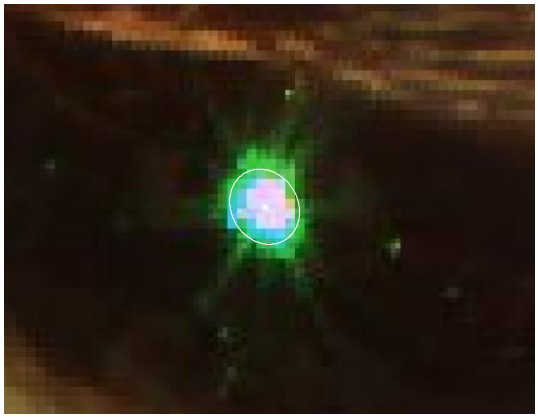

Figure 5. SC image with Segmented Elliptical region and Intensity-Weighted Centroid

Step 3 generates a single point from the segmented region. We fit an ellipse around the region and compute the intensity-weighted centroid of this ellipse. Figure 5 shows the result of this computation. Step 4 generates a 3D point by triangulating the 2D points of the left and right camera images. This is done by using the camera setup's intrinsic parameters such as focal length, camera center, and distance between cameras. Finally we repeat this entire procedure for each set of images that we collected.

3D Ultrasound Segmentation

Figure 6 shows the software pipeline for segmenting the PA signals from the 3D US volume. Step 1 is based on an intensity threshold filter. The 3D US volume is normalized and the pixels less than 0.3 are set to 0 and the pixels greater than or equal to 0.3 are set to 1. We acquired this threshold experimentally and it has been applicable to all of the data sets that we have collected. In step 2, we project the 3D volume onto a 2D plane along the axial direction of each slice. We use the mean intensities along each axial ray. Figure 7 shows an example of a mean intensity projected image. Step 3 segments the region by finding the region that most represents an ellipse and is within a pixel range. This pixel range was chosen experimentally and will vary based on the beam size. Step 4 computes the intensity-weighted centroid of a fitted ellipse. Figure 7 also shows the fitted ellipse and the computed centroid. Step 5 is where the axial point is determined. Based on the centroid which gives us the lateral

and elevational coordinates, we find the axial points at the 4 pixel locations forming corners surrounding our coordinate. These axial points are defined as the point of the PA signal that is closest to the surface. As mentioned before, there is non-zero penetration of the PA signal, but we are only interested in the surface signal. Thus, we can exploit this and use the surface-most PA signal. We then do a bilinear interpolation of the 4 axial coordinates to obtain our final PA signal point. These steps are repeated for every 3D US volume collected.

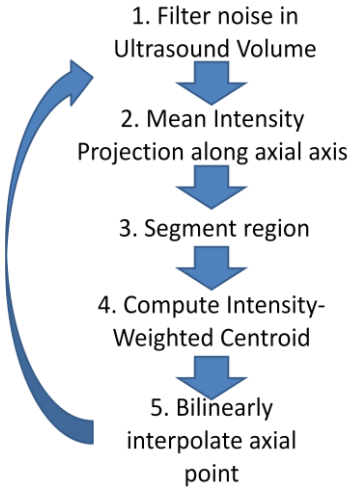

Figure 6. Software Pipeline for Segmentation of PA signal in 3D US

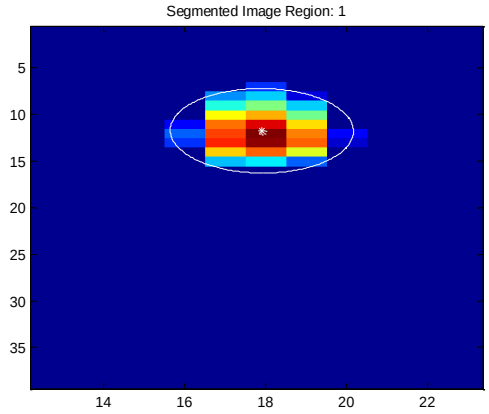

Figure 7. Zoomed-In Mean Intensity Projection Image with Ellipse and Intensity-Weighted Centroid

Registration

Figure 8 shows the software pipeline to compute a rigid registration between the two 3D point sets and the corresponding TRE for each test point. Step 1 is where a test point is removed from each data set. This test point will be used later to obtain the TRE. In step 2, a rigid registration based on Arun's algorithm [14] is obtained from the two 3D point sets. In step3, we transform the test point from step 1 from SC space to US space based on the registration from step 2. Finally, step 5 computes the TRE between the transformed SC test point and the corresponding PA signal point in 3D US space. This process is repeated where each data point is used as the test point.

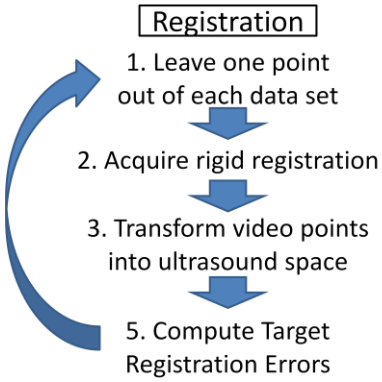

Figure 8. Software Pipeline for Registration

Visualization

We have two ways of visualizing the accuracy of our registration. The first is to plot the transformed SC points and the PA signal points in the 3D US space. This allows us to directly look at how the two point sets compare as ideally, they will be identical. Figure 10 is an example of one such plot and will be shown in the results section.

The alternate method for visualizing our registration is by transforming a representation of a US slice into the SC space. Figure 9 is an example of this image overlay.

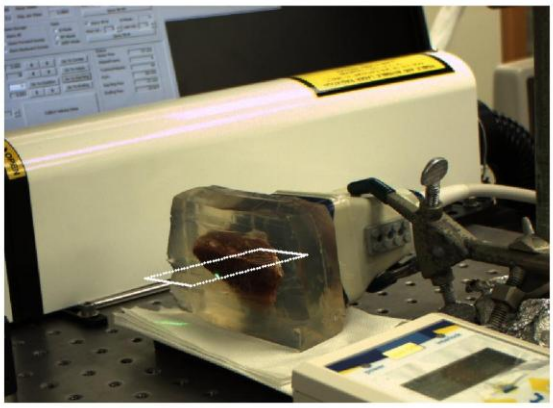

Figure 9. SC Image Overlaid with Representation of an US Slice

3. Results

We present 2 sets of results corresponding to a synthetic phantom and an ex-vivo liver tissue phantom. The numbers of test points are 30 and 33 respectively. Figures 10 and 11 correspond with the aforementioned visualization of both point sets within the 3D US space.

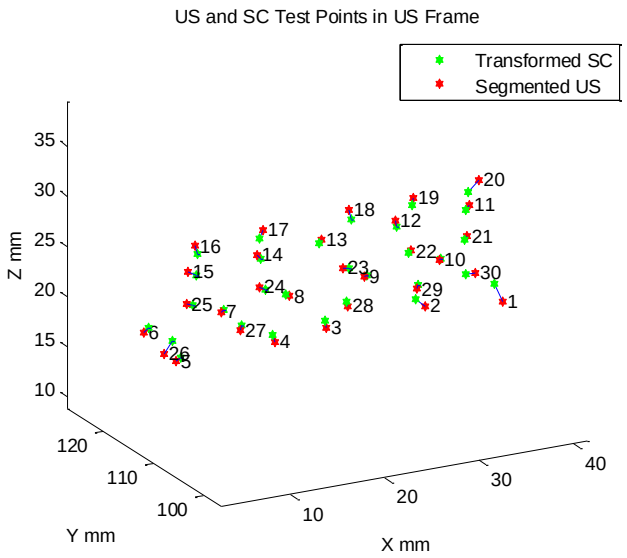

Figure 10. US and SC point sets in 3D US space for Synthetic Phantom Experiment

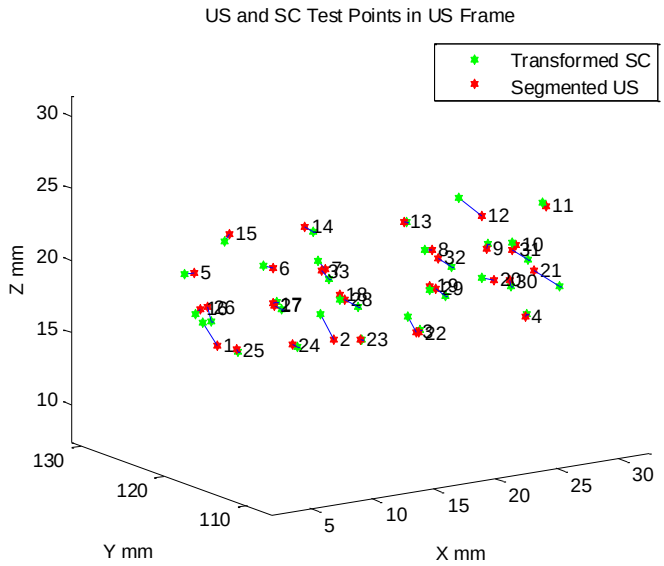

Figure 11. US and SC point sets in 3D US space for Ex-vivo Tissue Phantom Experiment

Table 1 shows the TRE for the synthetic phantom and ex-vivo tissue phantoms in each direction and the overall Euclidean error.

Target Registration Error		
Dimensions	Synthetic Phantom	Ex-Vivo Tissue Phantom
X-Lateral (mm)	0.39	0.28
Y-Axial (mm)	0.24	0.95
Z-Elevational (mm)	0.55	0.29
Euclidean (mm)	0.80	1.08

Table 1. TRE for Synthetic Phantom and Ex-Vivo Tissue Phantom Experiments

4. Discussion

We have shown results in table 1 that are significantly better than the errors reported for standard surgical guidance systems. They report errors of around 3 mm whereas we are reporting errors around 1 mm. The lateral error is only limited by the US resolution and has a bound of 0.3 mm. We are already extremely close to this bound with little room for improvement. The axial error also depends on the US resolution. This should theoretically be very low as there are many samples in the axial direction of a US image. Depending on the US sampling rate and image depth, the axial error bound should be in the order of 0.1 mm. We note that the errors we report are significantly larger than this number. This is because the axial error corresponds with the depth in the SC image. The depth is affected very significantly by any errors in SC segmentation. An error of 1 pixel corresponds to a depth error of 1 mm. We also note that this axial error is much higher in the ex-vivo tissue experiment than the synthetic phantom experiment. We believe that this is because the surface of the ex-vivo tissue is much more irregular than the synthetic phantom. In addition, if we look at figure 11, we can see that there are several outliers contributing greatly to the axial error. Finally, the elevational error depends mostly on the gap between the slices or how finely we sample our volume. In our current setup, the gap between each slice is about 0.5 mm. This value is a rough estimate as the depth of the signal affects this greatly. We do not expect much more improvement in the elevational error with this setup. Alternatively, if we used a linearly actuated probe, we could reach a bound of 0.1 mm or even less depending on the accuracy of the motor.

5. Conclusion

We have shown a complete PA system for registering video with 3D US and results that best the clinical standard. The next step for this system is to prepare it for practical use in a clinical scenario, conduct more experimental studies, and integrate with surgical robots.

6. Acknowledgements

We would like to thank XiaoYu Guo, Nathanael Kuo, and HyunJae Kang for their help in setting up the system. We would also like to thank Dr. Taylor, Dr. Boctor, Dr. Kang, and Dr. Prince for their helpful guidance and criticism throughout the project.

7. Management Summary

This was a challenging project and required a lot of work to setup the system and get everything working together. We were consistently aware of our management plan and frequent meetings with our mentors kept our project running smoothly. Table 2 shows a list of the project milestones and their respective planned and actual completion dates. There were some delays throughout the project, with the most notable being the fiber delivery system. There were many iterations, but they did not provide the desired results. Otherwise, the milestones were completed and the project goal was met.

Milestone	Expected Completion	Actual Completion	Status
Phantom Construction	February 27, 2012	March 6, 2012	Done
Ex-Vivo Tissue Phantom Construction	February 27, 2012	February 21, 2012	Done
3D Ultrasound Segmentation	February 27, 2012	February 27, 2012	Done
Fiber Delivery System	March 5, 2012	May 28, 2012	Ongoing
Visualization	March 26, 2012	April 2, 2012	Done
Automatic US and SC Segmentation	April 16, 2012	May 7, 2012	Done
System Integration	May 7, 2012	May 7, 2012	Done

Table 2. List of Project Milestones and Status

Future Work

This system is highly innovative and there is certainly a lot of future work to be done. In the near future, we will finalize a fiber delivery system and synchronize the transducer motor actuation and laser point projection. We will also integrate our system with a surgical robot as endoscopic cameras can easily replace our current SC setup. Other work would include more experimental trials and in-vivo studies.

Lessons Learned

In addition to the experience gained from working with photonics, optics, and ultrasound, I learned that software pipelines often require many revisions. I also learned that it is a good idea to store intermediate processed data even if there is no current use for it. The project plan must be constantly revised. The most important lesson that I learned was to validate my results and algorithms more rigorously before presenting them to my mentors. I often found bugs and errors after the fact, but luckily fixing these gave me better results.

Division of Labor

Alexis was responsible for all aspects of the project.

8. Appendix

The code and documentation can be found on the project webpage.

References

[1] Vyas S. et al., “Intraoperative Ultrasound to Stereocamera Registration using Interventional Photoacoustic Imaging”. SPIE 2012

[2] Spike, B. “The Photoacoustic Effect”. Physics 325 Lecture Notes 2006

[3] Wang, Y., Butner, S., and Darzi, A., “The developing market for medical robotics," Procs. of the IEEE 94(9), 1763-1771 (2006).

[4] Taylor, R., Lavallee, S., Burdea, G., and Mosges, R., [Computer integrated surgery], MIT Press Cambridge, MA (1996).

[5] Stolka P. J., Keil M., Sakas G., McVeigh E., Allaf M. E., Taylor R. H., and Boctor E. M., "A 3D-elastography-guided system for laparoscopic partial nephrectomies", in Medical Im-aging 2010: Visualization, Image-Guided Procedures, and Modeling, San Diego, Feb 13-18, 2010. pp. 76251I-76251I-12.

[6] Boctor E., Viswanathan A., Choti M., Taylor R., Fichtinger G., and Hager G., “A Novel Closed Form Solution for Ultrasound Calibration”. ISBI 2004

[7] Poon T., and Rohling R., “Comparison of calibration methods for spatial tracking of a 3-D ultrasound probe”. Ultrasound in Medicine and Biology August 2005, vol. 31(8): 1095-1108

[8] Navab N., Mitschke M., and Schutz O., “Camera-Augmented Mobile C-Arm (CAMC) Ap-plication: 3D Reconstruction using Low Cost Mobile C-Arm”. MICCAI 1999, 688-697

[9] Wiles A., Thompson D., and Frantz D., “Accuracy assessment and interpretation for optical tracking systems”. Medical Imaging 2004, vol. 5367: 421-432

[10] Kolkman, R., Steenbergen, W., and van Leeuwen, T., “In vivo photoacoustic imaging of blood vessels with a pulsed laser diode," Lasers in medical science 21(3), 134-139 (2006).

[11] Kuo, N., Kang, H., DeJournett, T., Spicer, J., and Boctor, E., “Photoacoustic imaging of prostate brachytherapy seeds in ex vivo prostate," in [Proceedings of SPIE], 7964, 796409 (2011).

[12] Xu, M. and Wang, L., “Photoacoustic imaging in biomedicine," Review of scientific instru-ments 77, 041101 (2006).

[13] Hoelen, C., De Mul, F., Pongers, R., and Dekker, A., “Three-dimensional photoacoustic im-aging of blood vessels in tissue," Optics letters 23(8), 648-650 (1998).

[14] Arun, K., Huang, T., and Blostein, S., “Least-squares fitting of two 3-d point sets," Pattern Analysis and Machine Intelligence, IEEE Transactions on (5), 698-700 (1987).

[15] Treeby B., and Cox B., “k-Wave: MATLAB toolbox for the simulation and reconstruction of photoacoustic wave-fields”. Journal of Biomedical Optics*.,* vol. 15, no. 2, p. 021314, 2010